Title: Thalamic state influences timing and feature selectivity in the thalamocortical circuit

Authors: Clarissa J Whitmire, Yi Juin Liew, Garrett B Stanley

Affiliation: Wallace H Coulter Department of Biomedical Engineering, Georgia Institute of Technology and Emory University, Atlanta, GA.

Contact info: Correspondence should be addressed to:
Professor Garrett B. Stanley
Coulter Department of Biomedical Engineering
Georgia Institute of Technology & Emory University
313 Ferst Drive
Atlanta, GA 30332
Phone: 404.385.5037
Email: Garrett.stanley@bme.gatech.edu

Keywords: thalamocortical, feature selectivity, thalamic state, burst/tonic

Acknowledgements: Confocal imaging was performed at the Georgia Tech IBB Imaging Core. We thank Peter Y Borden, Christian Waiblinger, and Aurélie Pala for helpful comments on the data analysis and manuscript.

Author Contributions: Conceptualization, C.J.W. and G.B.S.; Formal Analysis, C.J.W.; Investigation, C.J.W. and Y.J.L.; Writing – Original Draft, C.J.W. and G.B.S.; Writing – Review & Editing, C.J.W., Y.J.L., & G.B.S.; Visualization, C.J.W.;

Declaration of Interest: The authors declare no competing financial interests.

Summary

Thalamic neurons dynamically encode sensory information in a state-dependent manner as a mechanism for gating information flow to the cortex. Here, we investigated the role of thalamic state on precise feature selectivity in the thalamocortical circuit of the rat vibrissa pathway. In thalamic neurons, tonic spike triggered averaging revealed clear feature selectivity, while the feature selectivity associated with burst spikes could not be recovered with this approach. These thalamic state dependent changes propagated to cortex such that the cortical feature selectivity was diminished during the optogenetically hyperpolarized (burst biased) thalamic condition. Further analysis revealed that the perceived loss of feature selectivity was likely not due to a true loss of stimulus selectivity but instead to changes in the precision of the temporal spiking in burst firing modes. Therefore, alterations to thalamic state enable a dynamic interplay between spike timing and spike rate that shapes stimulus encoding in the thalamocortical circuit.

Introduction

Sensory thalamus plays a critical role in gating information flow from our sensors in the periphery to sensory cortex, ultimately shaping how we perceive the world. Importantly, thalamic gating properties are not static, but instead vary dynamically through a range of modulatory mechanisms, including local membrane and synaptic properties (Wolfart et al., 2005), stimulus history (Whitmire et al., 2016), and neuromodulatory inputs from brainstem and cortex (Castro-alamancos, 2002; Mease et al., 2014). Although arising from different mechanisms, these modulatory inputs have the net effect of altering the baseline membrane polarization level in the thalamus, which we refer to here as “thalamic state”, which plays an important role in determining the encoding properties of the thalamic neurons that serve as primary inputs to sensory cortex. Perhaps most prominently, modulation of the baseline membrane potential in thalamic neurons enables distinct tonic and burst firing modes due to the selective engagement of low threshold calcium channels during prolonged hyperpolarization (Suzuki and Rogawski, 1989). In addition to their roles in thalamocortical oscillations (Steriade et al., 1993), it has long been posited that these two firing modes could be a mechanism for dynamically controlling information processing (Sherman 2001). At the thalamocortical synapse, spontaneous burst spikes are more effective at driving cortical spiking (Swadlow and Gusev, 2001) and evoke larger cortical depolarizations (Bruno and Sakmann, 2006) than tonic spikes. It has been proposed that both burst and tonic spikes carry stimulus information (Reinagel et al., 1999), but the relationship between burst and tonic firing in representing temporal stimulus information in tactile encoding remains unclear.

In the visual pathway, the role of thalamic state in sensory processing has identified distinct sensory selectivity associated with burst versus tonic firing (Alitto et al., 2005; Denning and Reinagel, 2005; Lesica and Stanley, 2004; Reinagel et al., 1999; Wang et al., 2007). The burst response can be reliably elicited across trials in response to sensory stimulation (Lesica and Stanley, 2004; Martinez-Conde et al., 2002; Wang et al., 2007) and the feature selectivity of the bursts are characterized by a prolonged inhibitory stimulus before the depolarizing input that occurs immediately prior to the spike onset. This demonstrated that bursting activity is not

just an indicator of state, but it is also repeatably evoked by the sensory stimulation and is present in the awake animal (Guido and Weyand, 1995). However, how these results extend to other sensory modalities, such as touch, and the implication for downstream sensory encoding remains unknown.

Here, we quantified the role of thalamic state on temporal feature selectivity in the thalamocortical circuit of the rodent whisker pathway by implementing a class of models that maps sensory inputs to observed neuronal activity. Specifically, we characterized neurons using a two-stage, linear-nonlinear framework, the first stage of which represents the sensory feature selectivity, and the second stage of which represents the overall sensitivity of the input-output relationship. This characterization was performed for neurons recorded extracellularly both in the ventro posterior-medial (VPm) thalamus and in layer 4 of primary somatosensory cortex (S1) in the fentanyl-anesthetized rat. For thalamic neurons, we found that tonic spiking was associated with clear whisker-stimulus feature selectivity consistent with previous findings (Petersen et al., 2008). However, analysis of burst firing suggested a lack of feature selectivity, a finding which was further confirmed using optogenetic hyperpolarization of VPm to switch the thalamus into a burst state. An assessment of the temporal precision of the sensory-driven thalamic firing identified an increase in the timing jitter of burst spikes relative to tonic spikes that could underlie the differences in the recoverability of the feature selectivity. In the cortical neurons, we found that when thalamus was dominated by tonic firing, the cortical neurons exhibited similar feature selectivity as observed in VPm. However, when the thalamus was optogenetically hyperpolarized to push the local thalamic population further into a burst firing mode, this had a detrimental effect on the spike time precision of the downstream cortical neurons as well as the feature selectivity reflected by the model. Given the sensitivity of the thalamocortical circuit to precise timing of thalamic projection neurons, the results here suggest an important relationship between thalamic state, or membrane polarization, and the dynamic regulation of timing fidelity across thalamic firing modes that could have profound implications for coding during varying behavioral conditions.

Methods

Experimental Procedures

Acute Surgery: All procedures were approved by the Georgia Institute of Technology Institutional Animal Care and Use Committee and were in agreement with guidelines established by the National Institutes of Health. 19 female albino rats (Sprague-Dawley, 250-300g) were anesthetized intravenously using a fentanyl cocktail (fentanyl (5 μg/kg), midazolam (2 mg/kg), dexmedetomidine (150 μg/kg)). A craniotomy was performed over VPm (2-4 mm caudal to bregma, 1.5-3.5 mm lateral to the midline), and in a subset of animals, a second craniotomy was performed over S1 (1-3 mm caudal to bregma, 4.5-6 mm lateral to the midline). At the termination of the experiment, the animal was euthanized with an overdose of sodium pentobarbital (euthasol, 0.5 mL at 390 mg/mL). All optogenetically transfected animals that underwent cortical probe recordings were perfused and their brains were imaged for verification of opsin location and cortical probe location.

Electrophysiology: Tungsten microelectrodes were lowered into the thalamus (depth: 4.5-6 mm) using either a micropositioner (Kopf, Luigs-Neumann). Multielectrode probes (A1x32-10mm-50-177, NeuroNexus) were lowered perpendicular to S1 (45° relative to vertical; depth: 2 mm). The topographic location of the electrode was identified through manual stimulation of the whisker pad. Upon identification of the primary whisker for the recorded unit(s), the primary whisker was threaded into the galvo motor to permit stimulation of a single whisker.

Sensory Stimulus: Mechanical whisker stimulation was delivered using a precisely controlled galvo motor (Cambridge Technologies, custom Matlab software). The mechanical stimulus applied to the whisker in the rostral-caudal direction consisted of sensory white noise (low pass filtered at 200 Hz, standard deviation of the noise was 0.6° or 223°/s). Feedback from the whisker stimulator were used for further spike triggered analysis across all units (down sampled to 4.88 kHz).

Optogenetics surgeries: All surgical procedures followed sterile protocol. A small craniotomy was made above VPm (3 mm lateral, 3 mm caudal to bregma). A 10 µL syringe (Neuros Syringe, Hamilton, Inc) filled with the virus (rAAV5-CamKIIa-Jaws-KGC-GFP-ER2 or rAAV5-CamKIIa-eNpHR3.0-EYFP, UNC Viral Vector Core Services) was lowered to depth of 5.2 mm before injecting 1 µL of virus at a rate of 0.2 µL/min (iSi system, Stoelting). The syringe remained in place for five minutes after the injection was complete to allow the virus to diffuse. Opsin expression was fully realized at 2-3 weeks post-surgery.

Optogenetic Stimulus: Optical manipulation was administered with a controlled pulse of light through a custom optrode consisting of an optical fiber (200µm diameter; Thorlabs) and an electrode (Tungsten microelectrode; FHC) that was lowered into the VPm. Upon identifying a whisker sensitive cell, light sensitivity was assessed by the post-inhibitory rebound spiking response using a train of 250 millisecond light pulses (λ = 590 or 617nm for Halorhodopsin and Jaws, respectively). The whisker was then stimulated without (baseline) and with (hyperpolarized) light provided directly to the thalamus (50 mW/mm^2). Optogenetic stimulus conditions (light on/hyperpolarized, light off/baseline) were interleaved to avoid long-term adaptation effects.

Analytical Methods: Spike sorting for single channel recordings was performed online and validated offline using Waveclus (Quiroga et al., 2004). Spike sorting for multichannel electrodes was performed offline using the KlustaKwik software suite (Rossant et al., 2015). Isolation of the unit was confirmed by the waveform amplitude (absolute and relative to the background noise >3) and the interspike-interval distributions (VPm: mean of 0.22%, S1: mean of 0.38% of spikes in absolute refractory period of 1ms).

Feature selectivity was estimated for each recorded unit using the spike triggered average (STA) (Schwartz et al., 2006).

$$STA = \frac{1}{N}\sum_{j} s(t_j)$$

Where N is the number of spikes and s is the stimulus segment in a window surrounding each spike (-30 to +5 ms, spike-triggered ensemble, STE). The burst and tonic triggered averages were computed from burst and tonic spikes, respectively. The baseline/hyperpolarized condition triggered averages were computed from all spikes in a given stimulus condition. The bootstrap estimate of the confidence intervals on the spike triggered average was computed as the +/- 2 standard deviation of this shuffled STA distribution across 500 repetitions (Schwartz et al., 2006). Note that we implemented multiple techniques of estimating the feature selectivity of the neurons including spike triggered covariance, generalized linear models, and nonlinear-input models (McFarland et al., 2013). The results were qualitatively consistent across all methods employed, so we chose to use spike triggered average throughout the manuscript due to its simplicity.

The signal-to-noise ratio of the recovered STA was quantified as the peak-to-peak amplitude of the STA within 10 milliseconds of the spike (where the significant filter activity is contained) divided by the peak-to-peak amplitude of the STA from 30 to 20 milliseconds before the spike (where there is no expected filter information). An SNR value of 1 means the amplitude of the STA near the spike time is not different from the amplitude of the noise fluctuations. Therefore, any units with an SNR value less than 2 were excluded from further analysis.

To make comparisons of the feature selectivity across the population of recorded neurons, we computed a principle component analysis of the recovered STA (Estebanez et al., 2012). The first two principle components accounted for the majority of the variance (71.8% VPm, 78.4% S1).

The non-linearity ($P(spike|y)$) was estimated as the ratio of the probability of spike-trigged stimuli ($P(y|spike)$) to the probability of any stimulus segment in the stimulus ($P(y)$) multiplied by the mean firing rate of the neuron($P(spike)$) (Schwartz et al., 2006):

$$p(spike|y) = p(spike)\frac{p(y|spike)}{p(y)}$$

144 Where y is defined as the stimulus (s) convolved with the feature selectivity of the unit (STA)
145 (Lesica et al., 2007), referred to as filtered stimulus. For all conditions, the STA was defined
146 as the baseline or tonic spike triggered average. Throughout the manuscript, we separate the
147 firing rate (p(spike)) from the shape of the non-linearity (p(y|spike)/p(y)) to avoid confounding
148 differences in firing rate with differences in tuning.

149 The precision in the noise evoked firing was estimated for each spike classification (tonic,
150 burst, baseline, hyperpolarized). The precision was defined as:

151 $$precision = \sum_{n=-1}^{+1} \tau_{jitter}(n)$$

152 Or the number of spikes with τ_{jitter} values of +/- 1 ms duration normalized by the total number
153 of spikes. τ_{jitter} is defined for each spike as the temporal lag (t_{lag}) for the peak correlation
154 between the STA and the stimulus segment surrounding that spike (-30 ms to +5 ms).

155 $$\tau_{jitter} = arg \max_{t_{lag}} correlation\left(STA, s(t_j)\right)$$

156 The τ_{jitter} distribution was normalized by the total number of spikes in each condition (tonic,
157 burst, baseline, hyperpolarized).

158 All pairwise statistical comparisons were computed using a Wilcoxon signed rank test unless
159 otherwise noted.

Results

Feature selectivity is conserved across the thalamus and cortex

We recorded thalamic and cortical extracellular spiking activity in response to sensory white noise stimulation of a single whisker in the vibrissa pathway of the fentanyl-anesthetized rat (Figure 1A, see Methods). We estimated the feature selectivity for each unit as the spike triggered average (STA), which captures the features of the sensory stimulus that tended to precede spiking, and the static, point nonlinearity, which captures the translation into suprathreshold spiking activity (Figure 1B; see methods). Although this quantification was performed on longer unique noise segments, we also recorded the response to short (4-10 second) frozen white noise segments to examine the response across trials. Figure 1C shows an example recording from a simultaneously recorded pair of neurons in topographically aligned regions of the thalamus (left column, ventral posteromedial nucleus, VPm) and cortex (right column, primary somatosensory cortex, S1) in response to the repeated presentation of a single frozen white noise segment (top of each column). Across trials, the repeatability of the response to the noise stimulus is apparent in the raster plot, with clear vertical patterns across trials. The STA was computed for the thalamic and cortical unit for stimulus segments from -30 milliseconds prior to the spike to +5 milliseconds afterwards at a 0.2ms resolution (Figure 1C, bottom. The black dotted line indicates the time of the spike). The VPm STA shows clear feature selectivity in the 10-15 milliseconds prior to the thalamic spike as evidenced by the large amplitude of the STA relative to the shuffled case (grey confidence intervals). Beyond 15 milliseconds prior to the spike, the VPm STA is essentially flat and within the confidence bounds on the shuffled process. This suggests that, on average, the thalamic unit is only sensitive to the stimulus occurring in the previous 10-15 milliseconds. The S1 unit also displays feature selectivity as evidenced by the shape and amplitude of the S1 STA immediately prior to the cortical spike relative to the shuffled case. Although the VPm STA is nearly ten times as large in amplitude as the S1 STA, the similarity in the temporal dynamics can be visualized by shifting the VPm STA by 2 milliseconds relative to the S1 STA (Figure

187 1C, bottom, S1 STA black, VPm STA shifted by 2 milliseconds and scaled by a factor of 0.1

188 as grey dashed line).

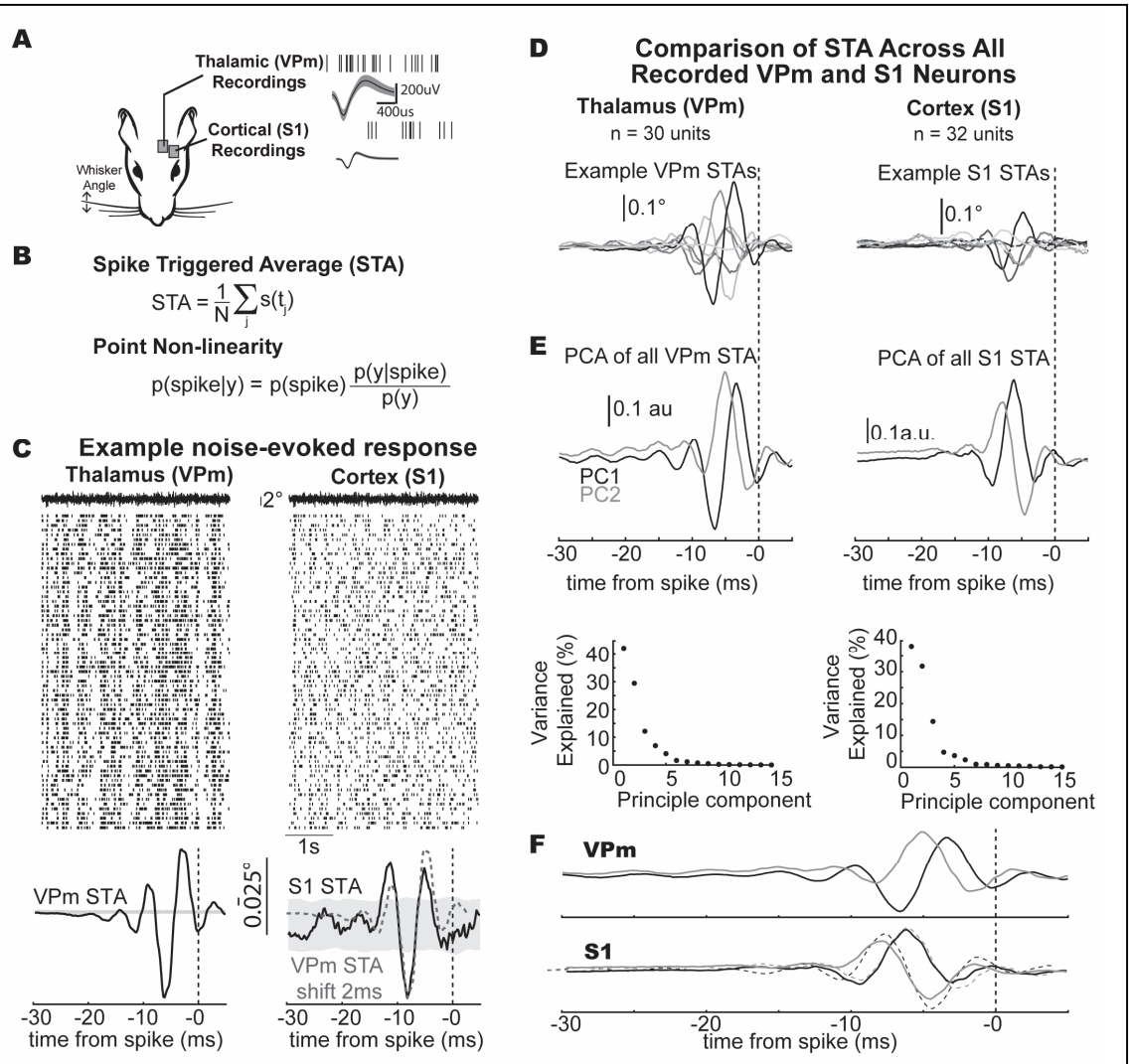

Figure 1: Feature selectivity in the thalamocortical circuit of the rat whisker pathway. A. Experimental paradigm. B. Feature selectivity is assessed from the neural response to sensory white noise as the spike triggered average and the associated point nonlinearity. C. Example noise evoked response from simultaneously recorded topographically aligned pair of neurons. D. Representative example thalamic and cortical STA (grey scale shows different examples). E. Principle component analysis (PCA) of all recovered STA for thalamic neurons and cortical neurons. F. Overlay of cortical STA PCs and temporally shifted thalamic PCs (shift of 2.5ms).

189 While this simple comparison provides an interesting observation for a single pair of

190 topographically aligned neurons, we also made comparisons of the feature selectivity across

191 the population of recorded STA for thalamus and cortex. First, we visualized the shape of the
192 spike triggered average for a sample of example thalamic (Figure 1D left; greyscale) and
193 cortical (Figure 1D right; greyscale) units. These STA filters cannot be simply averaged
194 together to give an estimate of the population filter due to differences in the phase and
195 directionality of the recovered STA across different recorded units. Instead, we performed a
196 principle component analysis on the set of recovered thalamic and cortical STA filters across
197 recordings to identify salient filter properties that generalized (Figure 1E). The first two
198 principle components for the spike triggered averages of both thalamus and cortex explain the
199 majority of the variance for the set of recovered filters, similar to what has been seen previously
200 for cortex (Estebanez et al., 2012). Furthermore, a simple time shift of 2.5 milliseconds for the
201 VPm principle components relative to the S1 principle components (Figure 1F, dashed lines)
202 demonstrates the similarity in the STA subspace spanned by these principle components. It
203 seems that despite not necessarily being recorded simultaneously or even in the same animal,
204 there is a high degree of overlap in the low dimensional subspace of feature selectivity for
205 thalamocortical neurons in the whisker pathway.

206

207 Tonic and burst spike feature selectivity in thalamus

208 Inherent in the spike triggered analysis, however, is an assumption that the average
209 filter is representative of the sensory stimulus preceding all spikes (Stanley, 2002). Yet
210 neurons in the thalamus are well known for exhibiting two fundamentally different types of
211 firing: tonic spiking and burst firing mediated through T-type calcium channels (Suzuki and
212 Rogawski, 1989). Burst spikes were classified here from the extracellular recordings as two
213 or more spikes with an inter-spike interval of less than four milliseconds with the first spike in
214 the burst preceded by 100 milliseconds of silence (Figure 2A, see methods). Using this

classification, we asked if or how the feature selectivity of an individual thalamic unit changes as a function of the spiking mechanism in the whisker pathway.

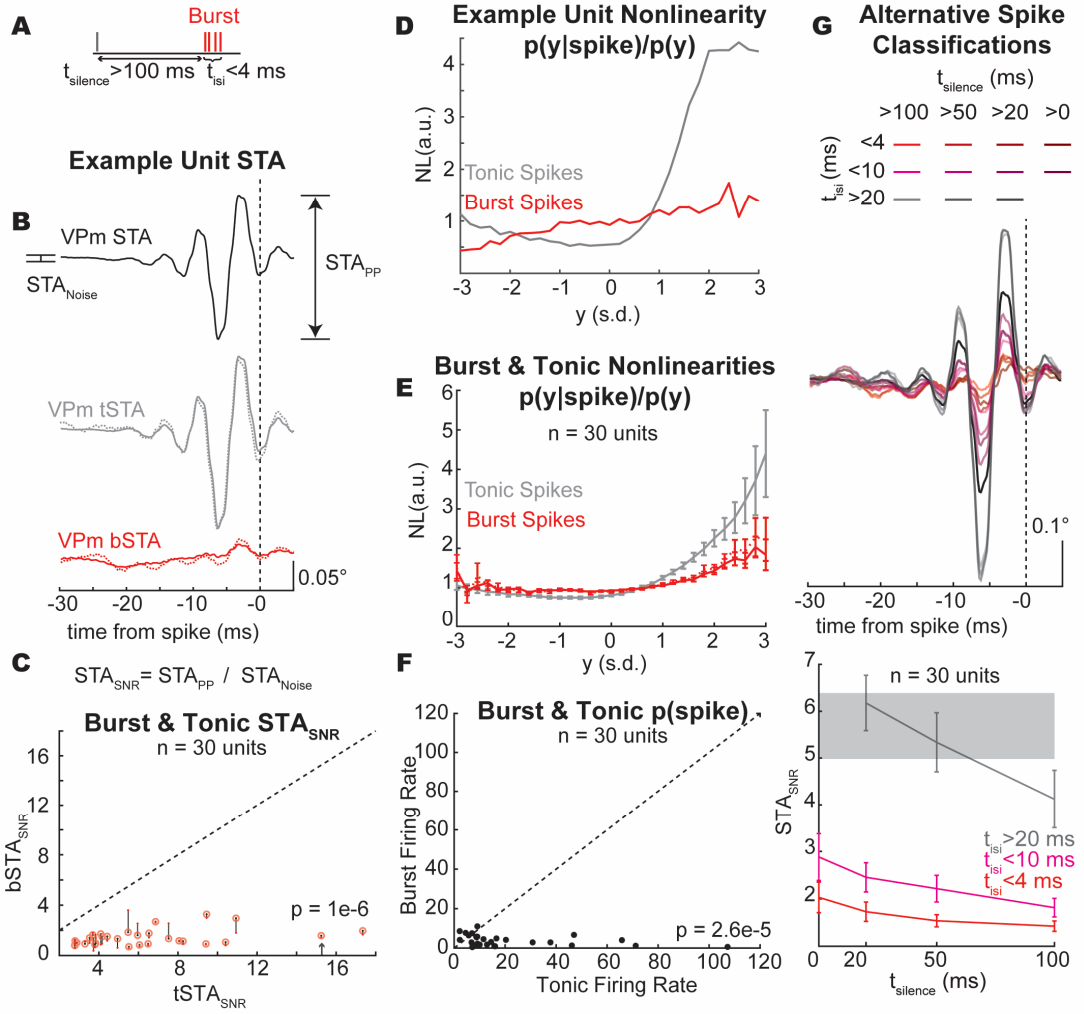

Figure 2: Feature selectivity of burst and tonic spikes in thalamic neurons. A. Burst definition. B. STA from thalamic unit presented in Figure 1 estimated from all spikes (black solid line, n = 44105 spikes), tonic spikes (tSTA; grey solid line, n = 36558 spikes), a subsample of tonic spikes (tSTA; dashed line, n = 2363 of 36558 spikes) all burst spikes (bSTA; red solid line, n = 7547 spikes), and the first spike in the burst (bSTA; red dashed line, n = 2363 spikes). C. STA_{SNR} across recorded population (n = 30 units). Black dots depict the STA_{SNR} for all bSTA computed from all burst spikes while red circles indicate the STA_{SNR} for bSTA computed from only the first spike in the burst (p = 1e-6). Arrow depicts example unit in A. D. Example unit tonic and burst spike nonlinearity. E. Average non-linearity across all units. F. Burst and tonic firing rate (p(spike)) across recorded population (p = 2.6e-5). G. Spike triggered average using different spike classifications.

In the thalamic recordings, tonic and burst spikes were interspersed throughout most of the recordings. For the example thalamic unit presented in Figure 1B, we computed the spike triggered average from all spikes (STA), the tonic spike triggered average from only tonic spikes (tSTA), and the burst spike triggered average from only spikes that are classified as being part of a burst (bSTA) (Figure 2B). The tSTA (grey) closely resembles the STA computed from all spikes (black) while the bSTA (red) is significantly degraded as evidenced by the flat shape of the filter. To compare the difference between burst and tonic feature selectivity across thalamic units, we quantified the signal-to-noise ratio of the STA (STA_{SNR}, see methods). Across all thalamic units, the SNR_{STA} was higher for tonic spikes ($tSTA_{SNR}$) than for burst spikes ($bSTA_{SNR}$) (Figure 2C).

Given the estimated feature selectivity, we can compute the static non-linearity, or the input-output function, which provides a mapping between this filtered stimulus (y) and the spiking response of the neuron (p(spike|y)) by taking the ratio of the p(y|spike) to the p(y) (Figure 1B, see methods). Here, we used the tSTA as the filter for all spiking conditions when estimating the non-linearity. The probability of the filtered stimulus (p(y) remains unchanged when the filter is held constant. Therefore, any change in the non-linearity is then only due to changes in the probability of the filtered stimulus given that a spike occurred (p(y|spike)), or the spike triggered ensemble. Because the slope of the static non-linearity is determined by the separation between the spike triggered ensemble and the Gaussian distributed white noise, as the spike triggered ensemble distribution becomes more selective (i.e. the mean moves away from the filtered stimulus distribution), the separability of the distributions increases, and the slope of the non-linearity also increases. Intuitively, this means that the shape of the non-linearity gives an estimate of the separability of the spike triggered ensemble and the stimulus distribution, or how strongly tuned a neuron is for that particular feature, given by the STA. A steeper slope in the non-linearity suggests a stronger tuning than a shallower slope. Therefore, we also assessed the spiking nonlinearity as a function of the spike classification. In this example unit, we found that the tonic spikes were well tuned to the STA,

as evidenced by the steep slope of the non-linearity while the burst spikes were not well tuned to the STA, as evidenced by the relatively flat non-linearity (Figure 2D). This trend was consistent across units where the burst spikes showed reduced tuning to the STA as compared to tonic spikes as assessed by the slope of the spiking nonlinearity (Figure 2E). Here, we have separated the difference in the slope of the non-linearity from the difference in the prevalence of burst and tonic spikes (p(spike)), which is markedly higher for tonic spikes than for burst spikes (Figure 2F). Furthermore, we tested alternative burst spike classifications and quantified the implication for the STA (Figure 2G, top). Across spiking classifications, increased periods of silence prior to the spike ($t_{silence}$) led to decreased STA_{SNR} while bursts of spikes (t_{isi}<4 or <10) had consistently lower STA_{SNR} relative to tonic spikes (t_{isi}>20) (Figure 2G, example unit in middle, population data in bottom). Therefore, our data do not provide evidence to support a difference in feature selectivity for tonic and burst spiking in this pathway, but instead suggests a reduction in stimulus selectivity in burst spiking within this analytic framework.

Thalamic state dependent feature selectivity

The previous analysis was conducted by presenting sensory white-noise stimuli and parsing measured thalamic spiking activity into tonic and burst classes, while these classes of spiking were intermingled throughout the recordings. However, the thalamus was in tonic firing mode, with relatively low burst firing rates (Figure 2F). Here, we used optogenetic hyperpolarization of the thalamic neurons not to silence the thalamic neurons, but instead to shift the thalamus into a burst firing mode during sensory white noise stimulation (Figure 3A). Using this optogenetic manipulation, we asked whether the optogenetically manipulated firing mode (baseline and hyperpolarized conditions) of the thalamus impacts feature selectivity and how this relates to the classified burst/tonic modes.

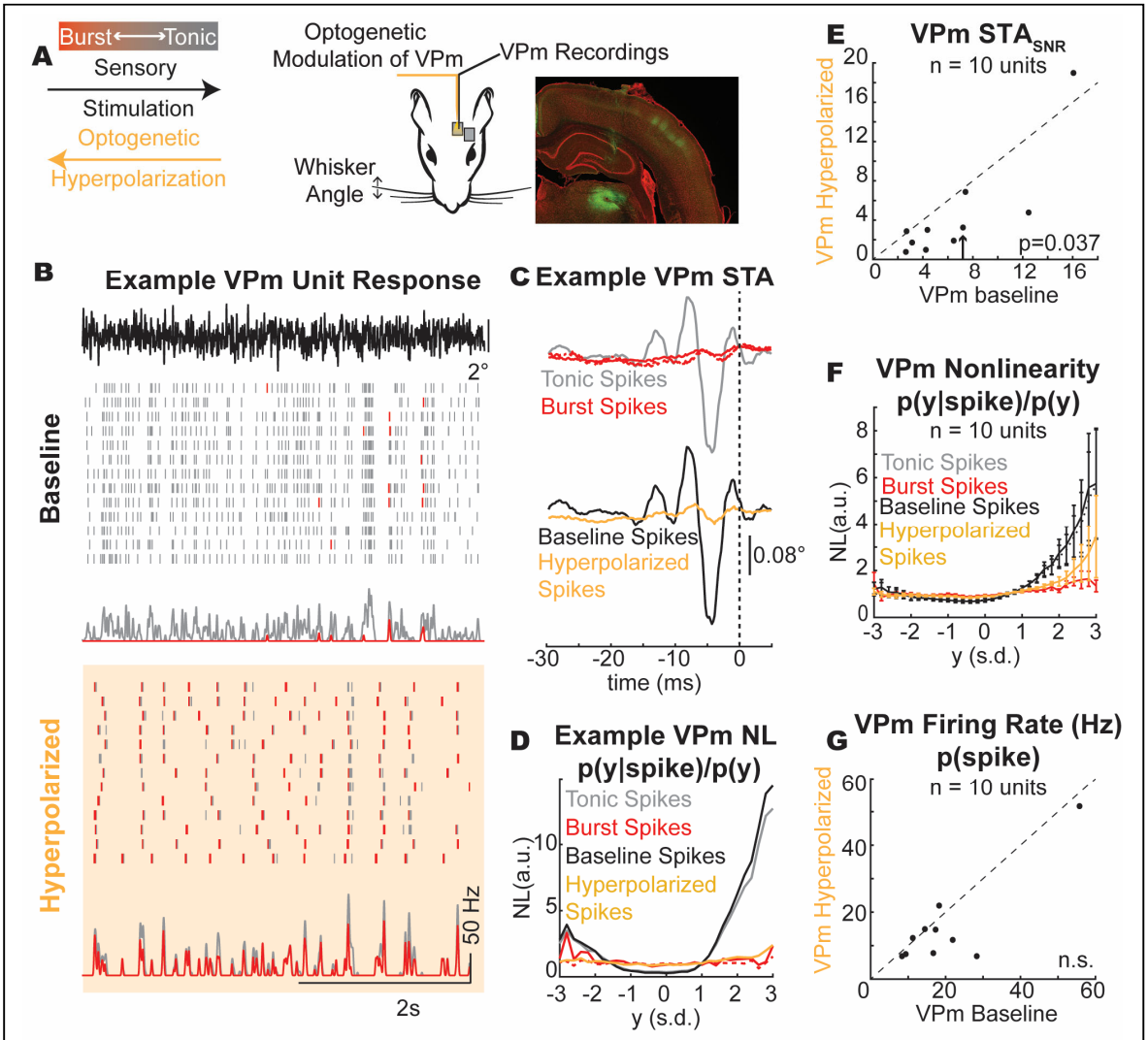

Figure 3: Optogenetic Manipulation of Thalamic State. A. Experimental paradigm. Scale bar: 1 mm. B. Example thalamic response to frozen white noise segments without (baseline) and with (hyperpolarized) optogenetic stimulation. C. Spike triggered average computed as a function of spike classification (burst, tonic) or thalamic state (baseline, hyperpolarized). D. Example unit tonic/burst and baseline/hyperpolarized spike nonlinearity. E. STA_{SNR} across recorded population (n = 11 units). Arrow depicts example unit in B. F. Average non-linearity across all units. G. Baseline and hyperpolarized firing rate (p(spike)) across recorded population (p>0.05).

Here, we recorded the thalamic response to sensory white noise with and without the presence of a light stimulus (hyperpolarized and baseline conditions, respectively) to shift the firing mode of the thalamus towards burst firing (baseline burst ratio = 0.16 ± 0.15, hyperpolarized burst ratio = 0.36 ± 0.27, n = 10 units). For an example unit, we have plotted

the spiking response to a frozen white noise segment without optogenetic stimulation (Figure 3B, baseline condition) and with optogenetic stimulation (Figure 3B, hyperpolarized condition). We have pseudocolored the tonic spikes grey and the burst spikes red to qualitatively visualize the thalamic firing mode (Figure 3B). In the baseline condition, the response is primarily tonic as evidenced by the grey raster plots (Figure 3B, Baseline, BR = 0.10). In the hyperpolarized condition (optically stimulated), the firing mode is biased towards a burst encoding scheme, as evidenced by the prevalence of red burst spikes (Figure 3B, Hyperpolarized, BR = 0.67). The tonic STA showed pronounced feature selectivity for this unit while the burst STA did not (Figure 3C top), consistent with the earlier findings (Figure 2). In the optogenetically manipulated states, the baseline STA has prominent feature selectivity while the hyperpolarized condition is much smaller in amplitude (Figure 3C bottom). Qualitatively, we can see that the STA from hyperpolarized condition reflected the STA obtained from the burst spiking in the previous analysis.

The similarity between the burst spike response and hyperpolarized condition can also be seen in this example nonlinearity where the burst and hyperpolarized nonlinearities are effectively flat while the tonic spikes and baseline condition show obvious tuning (Figure 3D). Across units, we found an overall reduction in the STA_{SNR} for the hyperpolarized condition relative to the baseline condition (Figure 3E, $p = 0.037$). We also found that the tuning of the nonlinearity was lower for the hyperpolarized condition relative to the baseline condition as reflected in the overall gain/slope (Figure 3F). Importantly, the baseline and hyperpolarized conditions both contain burst and tonic spikes. Instead of completely separating the firing modes into all burst spikes or all tonic spikes, we have optogenetically altered the spiking probabilities such that the baseline condition has more tonic spikes and the hyperpolarized condition has more burst spikes while maintaining similar numbers of spikes (Figure 3G). The similarities between the STA and the NL properties of the burst and hyperpolarized state as well as the tonic and baseline state suggest that there was no discernable difference for the

299 estimation of feature selectivity when assessed based on the state of the thalamus at the time
300 of the stimulus (hyperpolarized/baseline) versus the spike type classification (burst/tonic).

301

302 Temporal precision of thalamic firing modes

303 Given the difference between the recovered estimates of burst/hyperpolarized and
304 tonic/baseline feature selectivity, we implemented a series of computational controls to identify
305 any potential shortcomings of the methodologies that could underlie these results. The first
306 issue we considered was whether or not the burst spike feature selectivity was unrecoverable
307 due to the effect of subsequent spikes in the burst. If the timing of spikes within a burst is not
308 repeatable and structured, the presence of these additional spikes will serve to destroy the
309 temporal structure in the feature selectivity as revealed by the spike triggered analysis. When
310 the bSTA was computed from only the first spike in each burst (Figure 2B, red-dashed line),
311 there was no apparent feature selectivity for this example unit. This can also be visualized
312 across units in the STA_{SNR} where the $bSTA_{SNR}$ is plotted when computed from all burst spikes
313 (black dot) and when computed from the first spike in each burst (red circle, Figure 2C).
314 Therefore, including all spikes in a burst (or not) does not strongly impact the ability to estimate
315 the feature selectivity from the STA.

316 The second issue we considered was the overall difference in spike rates. Spike
317 triggered analyses require a large number of spikes to effectively estimate the underlying
318 selectivity. The proportion of spikes classified as bursts was lower than the spikes classified
319 as tonic (Figure 2F) as quantified by the burst and tonic firing rate. Therefore, it was possible
320 that we could not recover an STA for the burst spike condition due to the reduced number of
321 burst spikes relative to tonic spikes. In an example unit, we computed the tSTA using only a
322 subset of the spikes (n = 2362 of 36558 spikes corresponding to n = 2363 bursts with n =
323 7547 burst spikes) and found that the linear filter was essentially identical to the tSTA (Figure
324 2B, grey dashed line). We computed this for all thalamic units and again found that the burst-
325 count matched tSTA was also significantly larger than the bSTA. Furthermore, there was no

326 statistically significant difference in the firing rate between the baseline and hyperpolarized
327 optogenetic conditions (Figure 3G), but still the difference in the STA persisted. This suggests
328 that simple spike counts alone were insufficient to explain the difference in the tonic/baseline
329 STA and the burst/hyperpolarized STA.

330 The third issue we considered was the inherent assumption that the feature selectivity
331 for each unit could be recovered as the STA. It was possible that the burst STA was not
332 recoverable because the burst firing mode was better estimated by a symmetric nonlinearity
333 and therefore the filter could only be recovered using spike triggered covariance (STC)
334 techniques. We therefore computed the STC for all recorded thalamic units and compared this
335 for each spiking condition. Although the dataset was more limited because the number of units
336 with a significant STC filter was lower than those with a significant STA filter (n = 13 units with
337 STC filter compared to n = 30 units with STA filter), the same trends regarding the reduction
338 in the amplitude of the filter (STC_{SNR}) and the slope of the symmetric nonlinearity persisted
339 (data not shown). Therefore, this suggests that the method of extracting the feature selectivity
340 (STA compared to STC) was insufficient to explain the inability to estimate the feature
341 selectivity in the hyperpolarized/burst spiking conditions.

342 The fourth assumption made throughout the analysis was that burst spikes are actually
343 driven by sensory stimuli such that there is a recoverable burst spike feature selectivity. The
344 alternative explanation would be that burst spikes are not feature selective and instead occur
345 randomly due to intrinsic or other non-sensory processes. To assess this, we quantified the
346 trial-to-trial repeatability for bursts in response to frozen white noise segments. As can be seen
347 in Figure 3B, the qualitative assessment of temporally aligned bursts in response to the frozen
348 white noise segment suggests that the bursts are driven by the sensory stimulus in a
349 repeatable way. For units with a sufficient number of repeated trials, we computed the
350 reliability of the burst spiking as the correlation between the peristimulus time histogram of
351 even and odd trials in response to the frozen white noise segment. We found that all units
352 showed greater reliability than what is expected based on just the temporal correlations in the

353 burst spiking (shuffle control, p = 0.002, n = 10 thalamic units). This suggests that the bursts
354 are not randomly generated or due entirely to a non-stimulus related phenomenon.

355 From these controls, we propose that the difference in the spike triggered encoding
356 properties could not be attributed to differences in the overall spike rates, the temporal
357 properties of the spikes within the burst, or the mechanism of filter estimation. Instead, we
358 propose that the burst spikes are driven by the sensory stimulus and have an underlying
359 feature selectivity, but that this cannot be recovered using spike triggered techniques due to
360 the reduced temporal precision of burst spiking relative to tonic spikes.

361 Recovering an STA relies on precise temporal spiking relative to the sensory stimulus.
362 To simulate degradation of the spike timing precision, we added independent samples of
363 normally distributed temporal jitter of varying amplitudes (standard deviation of the jitter
364 distribution) to each tonic spike for an example unit and computed the STA (Figure 4A).
365 Across units, we quantified the degradation of the STA as the jittered-STA_{SNR} normalized by
366 the $tSTA_{SNR}$ (0 ms jitter). The jittered-STA_{SNR} (black) is within the band expected for the
367 $bSTA_{SNR}$ with the addition of 4 milliseconds of jitter to the spike times (red shaded, Figure 4A,
368 right). We propose that the effects of temporal jitter are particularly evident for whisker
369 selectivity, presumably due to the short temporal duration of the filters (approximately 10-15
370 milliseconds in duration, Figure 1F).

371 Given the marked effects of jitter on the ability to recover the STA, we investigated the
372 variability in the spike timing relative to the noise stimulus (Figure 4B). For this example unit,
373 we have identified a segment in the noise stimulus that closely resembles the tonic STA for
374 this unit and elicits a reliable spiking response (Figure 4B, top; stimulus – black, tSTA – grey
375 dashed). The vertical dashed line indicates the spike time for the spike triggered average (t_0)
376 with the grey bar indicating the duration of the STA. If there was no variability in the neural
377 spiking, the raster plots would all be perfectly aligned to t0 because the similarity between the
378 stimulus and the STA would predict a spiking response at that time point. However, the timing
379 of evoked neural responses is always variable to some extent and this can be visualized for

this example response segment as the temporal variability of the spike times surrounding this stimulus feature in the noise stimulus (Figure 4B, as indicated by the grey stimulus bars that extend from the first spike response to this particular sensory feature). For this example snapshot, it is also apparent that the burst spikes in the hyperpolarized condition show greater temporal variability than the tonic spikes in the baseline condition.

To quantify this jitter across all spikes, we developed a τ_{jitter} metric that determines the time lag of the peak correlation between the STA and the stimulus segment ($s(t_j)$) surrounding each spike (Figure 4C). Intuitively, this is a correlative method to identify the time lag between when we predict a spike is most likely to occur based on the STA and the stimulus (peak correlation) and when the spike actually occurred. For this analysis, we treated the tSTA as the true feature selectivity of the neuron across all spiking conditions because we could not recover a reliable estimate of the bSTA.

We computed τ_{jitter} for each spike and plotted τ_{jitter} distributions for each spike condition (tonic, burst, baseline, hyperpolarized). If a neuron was infinitely precise such that when the stimulus matched the spike triggered average, the neuron fired a spike without delay, this distribution would be represented by a delta function at τ_{jitter} equals zero. As the variability of the timing increases, the width of this distribution will also increase. For the tonic and baseline condition spikes, we found a clear peak in τ_{jitter} values at τ_{jitter} equals zero (Figure 4C, grey, black). For the burst and hyperpolarized condition spikes, we observe little-to-no peak in the τ_{jitter} metric at zero (Figure 4C, red, yellow). We computed the τ_{jitter} distribution across all thalamic units and found that the tonic and baseline spikes had higher peaks at τ_{jitter} equals zero than the burst and hyperpolarized spike conditions (Figure 4D). We quantified this statistically by computing a precision metric (Figure 4C) that computes the proportion of spikes within ±1 millisecond of τ_{jitter} equals zero (Figure 4E). The tonic and baseline spike condition were more precise than burst and hyperpolarized conditions.

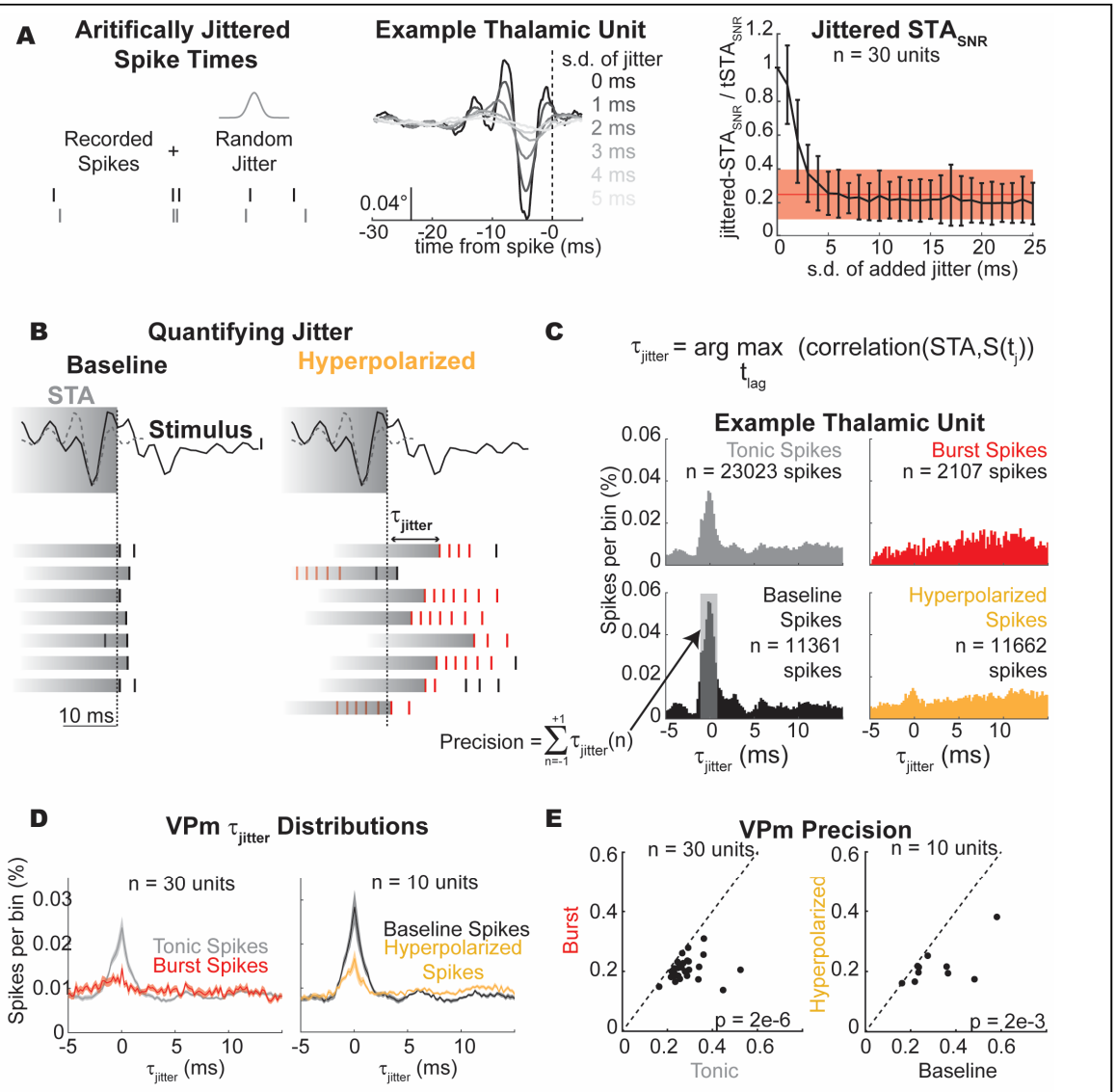

Figure 4: Thalamic timing variability in the response to the sensory white noise. A. Effect of increased jitter on thalamic STA (schematic: left, example: center). Across units, the normalized amplitude of the jittered STA (jitteredSTA$_{SNR}$/tSTA$_{SNR}$) was plotted across jitter intensities (black, right). The normalized amplitude of the burst STA (bSTA$_{SNR}$/tSTA$_{SNR}$) is shown in red (mean ± s.d.). B. In this example, the same stimulus (black; scale bar: 0.1°) was presented with and without optogenetic hyperpolarization (data from example unit presented in Figure 3 with associated STA (grey dotted line; scale bar: 0.025°)). C. Example unit τ_{jitter} distributions for burst, tonic, baseline, and hyperpolarized conditions. D. Average τ_{jitter} distributions for burst/tonic spikes (n = 31 units) and baseline/hyperpolarized condition (n = 11 units). (mean +/- sem). E. Precision for burst/tonic spikes (n = 31 units, p = 1e-6) and baseline/hyperpolarized condition (n = 11 units). (mean +/- sem, p=1e-3).

405

These data suggest that tonic spikes showed greater temporal precision in response to the sensory white noise than burst spikes and that this could underlie the difference in the recoverability of the feature selectivity in the thalamus between firing modes. It is well established that the timing of sensory inputs is particularly important in the thalamocortical circuit such that changes in thalamic spike timing could have large impacts on the downstream representation of sensory information in the cortex. Next, we investigated how these changes in temporal precision in optogenetically modulated thalamic states impact cortical encoding properties.

Optogenetic modulation of thalamic firing modes directly impacts cortical representation of sensory information.

Cortical neurons that receive direct thalamic input are integrating information over a population of thalamocortical neurons that can be operating in different firing modes. This makes it difficult to determine the impact of a single burst from a single neuron on information representation in the pathway. Instead, we used the optogenetic manipulation of thalamic state as presented in Figure 3 to bias the activity of the thalamic population towards burst firing (hyperpolarized condition) and investigated the effects on the cortex. Here, we transfected the thalamus with a hyperpolarizing opsin and lowered an optic fiber into the thalamus while recording the cortical activity extracellularly (Figure 5A) in response to sensory white noise with and without optogenetic manipulation of the thalamus (hyperpolarized VPm, baseline VPm).

For an example unit, we have plotted the cortical STA in the baseline and hyperpolarized VPm conditions (Figure 5B). Here, the amplitude of the cortical STA was smaller when the thalamus is hyperpolarized compared to when it is not (Figure 5B). This cortical unit also shows a reduced tuning to the STA when the thalamus was hyperpolarized (Figure 5C). Across the population of recorded cortical neurons, we saw the same effect seen in this example neuron of a reduced STA_{SNR} when the VPm was hyperpolarized compared to

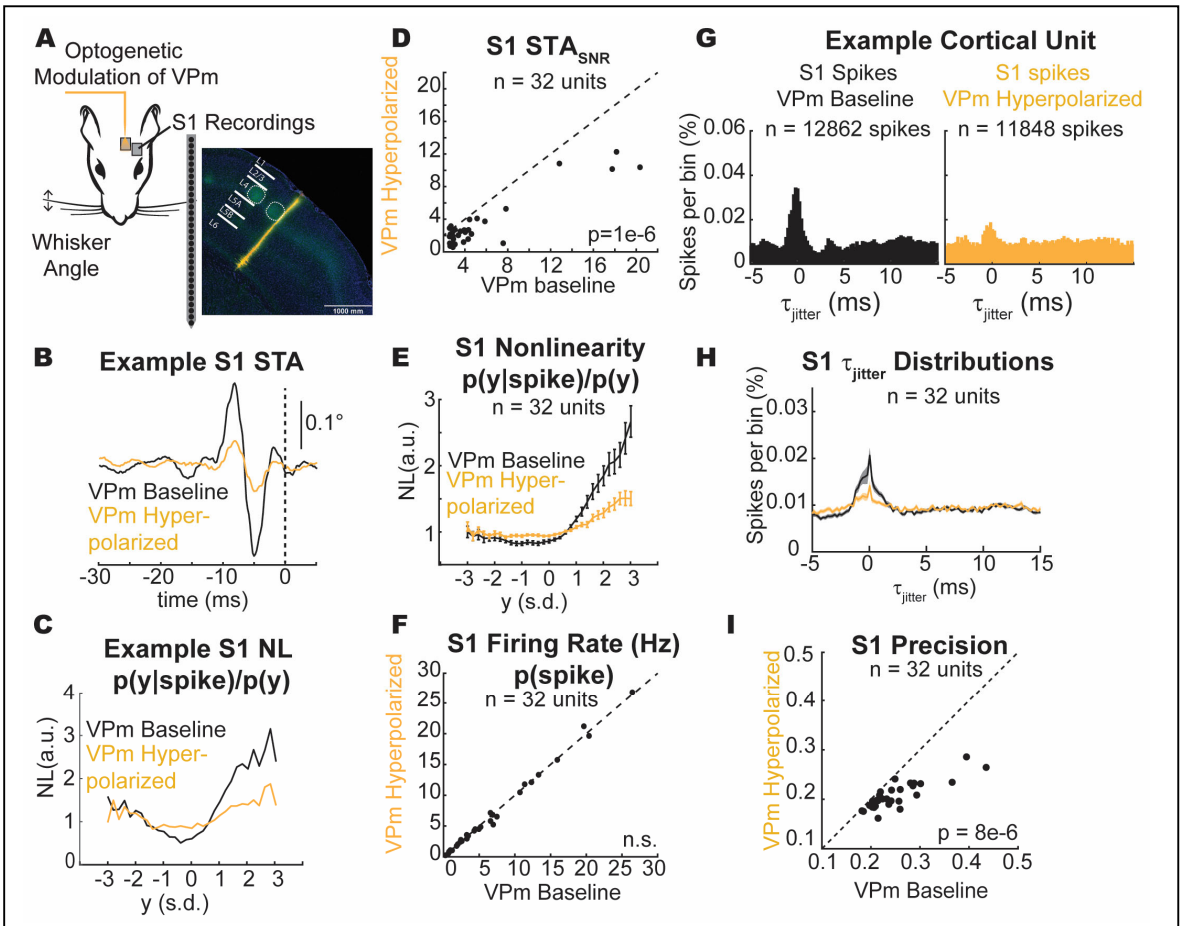

Figure 5: Optogenetic modulation of thalamic firing modes directly impacts cortical representation of sensory information. A. Experimental paradigm. Scale bar: 1 mm. B. Example STA for a cortical unit recorded during optogenetic manipulation of the thalamus. C. Example cortical nonlinearity as a function of thalamic state. D. STA_{SNR} across cortical units (n = 32 units. p = 1e-6). E. Spiking nonlinearity across cortical units. F. Cortical firing rate (p = 0.31). G. Example cortical unit τ_{jitter} distributions for baseline and hyperpolarized thalamic conditions. H. Average τ_{jitter} distributions for baseline/hyperpolarized thalamic condition (mean +/- sem). I. Precision for cortical spikes during baseline/hyperpolarized thalamic condition (mean +/- sem, p=8e-6).

433 when it was not (Figure 5D) and a reduction in the tuning across all cortical units as quantified
434 by the spiking nonlinearity (Figure 5E). These findings mirror what was seen for thalamic
435 neurons when comparing the baseline and the optogenetically manipulated conditions
436 demonstrating that the changes in thalamic encoding properties are propagated to cortex.

437 Interestingly, there was no significant difference in the noise-evoked firing rate in the
438 cortex as a function of the VPm condition (Figure 5F). This suggests that it was not overall
439 spike counts influencing the cortical feature selectivity. Instead, we propose the temporal jitter
440 in the thalamic spiking patterns propagated to cortex. We investigated the temporal precision
441 of the cortical spiking in response to the sensory white noise using the same methodology
442 employed for the thalamus. As we saw for the thalamus, the cortical spikes from this example
443 unit also showed greater temporal precision in the baseline VPm condition compared to the
444 hyperpolarized VPm condition (Figure 5G) as evidenced by the peak in the τ_{jitter} distribution
445 around τ_{jitter} equals zero. This effect was consistent across the population of recorded cortical
446 units (Figure 5H) and showed significant differences in the precision of the cortical firing
447 (Figure 5I). This suggests that the temporal jitter present in the thalamus is transmitted to the
448 cortex where it also impacts the representation of sensory information.

449

Discussion

The highly interconnected thalamocortical pathway dynamically gates information flow between the periphery and higher cortical centers dependent on many factors including behavioral state (Niell and Stryker, 2010), task demands (Atiani et al., 2009), and sensory adaptation state (Whitmire et al., 2016). Although there have been extensive investigations into the cortical state-dependent processing of the thalamocortical circuit, we know surprisingly little about how this information is processed in a thalamic state-dependent manner. Here, using a combination of optogenetic stimulation and electrophysiological recording techniques, we have performed a series of experiments modulating the state of the thalamus (through constant optogenetic hyperpolarization) and quantified the effects on encoding in the thalamocortical circuit. Using this technique, we have coarse control of the firing mode in thalamus without altering the processing occurring from the whisker to thalamus, enabling us to decouple the changes in thalamic firing mode on thalamocortical processing from changes occurring in subthalamic processing. We found that, unlike the visual pathway, the feature selectivity of burst spikes in the vibrissa pathway could not be recovered using spike triggered techniques due to increased burst spike timing variability relative to tonic spike timing. Recordings from barrel cortex during optogenetic manipulation of thalamic state demonstrated a shift in the temporal precision of the cortical spiking that also led to a degradation of the recovered feature selectivity. This suggests that bursts in the whisker pathway are less precise than tonic spikes during ongoing sensory stimulation and that this loss of temporal precision is propagated to cortex.

These results could be interpreted as consistent with the view that bursts are not representing detailed stimulus information. However, there is evidence that bursts may convey more information than the presence or absence of a burst through inter-burst spike timing and the number of spikes per burst (Mease et al., 2017), suggesting a role of temporally precise burst firing in information representation. Furthermore, thalamic bursting can be temporally precise within and across neurons in response to high intensity whisker stimuli (Whitmire et

al., 2016). Instead, we propose that the temporal precision of the thalamic firing is a function of both the state of the thalamus and the intensity of the sensory stimulus. It has previously been shown that the temporal precision of thalamic encoding increases with the intensity of the sensory stimulus (Desbordes et al., 2008; Whitmire et al., 2016) while here we have shown that the temporal precision of the thalamic firing decreases with sustained hyperpolarization. These two competing factors would enable the burst firing mode to encode high amplitude stimuli in a temporally precise fashion while low amplitude stimuli, such as the sensory white noise presented here, would not be able to overcome the variability present in the burst state.

There are multiple mechanisms that could underlie the reduced temporal precision in the burst firing mode including variability introduced by the slow dynamics of the calcium depolarization, increased variability in the time to reach threshold due to the prolonged hyperpolarization of the baseline polarization, as well as potential changes in the integration properties of the thalamic neurons. Furthermore, these mechanisms could occur independently such that the variability across neurons is uncorrelated or these mechanisms could be coordinated in some way to enable correlated variability across the thalamic population. Both coordinated and uncoordinated jitter would have a detrimental effect on the ability to recover the STA because either the spike timing would no longer be locked to the stimulus itself or the input to the cortex would be temporally imprecise. However, coordinated jitter would maintain the information about the stimulus while uncoordinated jitter would degrade the recoverability of the stimulus features. Future work should investigate the jitter in the burst spiking across units to determine whether or not the variability in the spike timing is coordinated across thalamic units in this context.

Given the importance of thalamic spike timing precision within and across neurons in transmitting information downstream to cortex (Bruno and Sakmann, 2006; Wang et al., 2010), alterations to thalamic state can shape multiple properties of the spiking inputs to cortex. Manipulation of the thalamic state can lead to changes in the stimulus evoked cortical dynamics (Whitmire et al., 2017) and spatiotemporal cortical activation (Borden et al., 2017).

We have primarily considered thalamic state-dependent encoding as a feedforward representation from thalamus to cortex, but the highly interconnected thalamocortical circuitry is a dynamic interaction that shapes coding properties in both feedforward and feedback manner. Changes in thalamic activity impact cortical activity which then provides feedback to thalamus to further alter activity (Crandall et al., 2015; Mease et al., 2014; Poulet et al., 2012; Reinhold et al., 2015; Wimmer et al., 2015). It is possible for thalamus to influence cortical state and for the cortex to influence thalamic state, but how this plays out during natural behaviors is not yet known and must be decoupled using more sophisticated techniques such as closed-loop control of neural activity (Bolus et al., 2018; Newman et al., 2015). The ability to shift the temporal precision of the thalamic spike timing through changes to the thalamic state, or the baseline membrane potential, provides a biophysical mechanism for the thalamus to gate information flow to cortex. Furthermore, this mechanism could be under both feedforward and feedback control. This sets the stage for a dynamic interaction between thalamic and cortical states to drive highly interactive patterns of neural activity.

518 **References**

519 Alitto HJ, Weyand T, Usrey WM. 2005. Distinct Properties of Stimulus-Evoked Bursts in the
520 Lateral Geniculate Nucleus. *J Neurosci* **25**:514–523. doi:10.1523/JNEUROSCI.3369-
521 04.2005

522 Atiani S, Elhilali M, David S V., Fritz JB, Shamma SA. 2009. Task Difficulty and Performance
523 Induce Diverse Adaptive Patterns in Gain and Shape of Primary Auditory Cortical
524 Receptive Fields. *Neuron* **61**:467–480. doi:10.1016/j.neuron.2008.12.027

525 Bolus MF, Willats AA, Whitmire CJ, Rozell CJ, Stanley GB. 2018. Design strategies for
526 dynamic closed-loop optogenetic neurocontrol in vivo. *J Neural Eng* **15**:026011.
527 doi:10.1088/1741-2552/aaa506

528 Borden PY, Kolb I, Ortiz AD, Sederberg AJ, Stoy W, Forest CR, Morrissette AE, Jaeger D,
529 Stanley GB. 2017. Thalamic control of sensory evoked spatiotemporal cortical
530 responses.2017 Neuroscience Meeting Planner. Washington, DC: Society for
531 Neuroscience, 2017. Online. p. 583.04.

532 Bruno RM, Sakmann B. 2006. Cortex is driven by weak but synchronously active
533 thalamocortical synapses. *Science* **312**:1622–7. doi:10.1126/science.1124593

534 Castro-alamancos MA. 2002. Properties of primary sensory (lemniscal) synapses in the
535 ventrobasal thalamus and the relay of high-frequency sensory inputs. *J Neurophysiol*
536 946–953.

537 Crandall SR, Cruikshank SJ, Connors BW, Crandall SR, Cruikshank SJ, Connors BW. 2015.
538 A Corticothalamic Switch: Controlling the Thalamus with Dynamic Synapses. *Neuron*
539 **86**:1–15. doi:10.1016/j.neuron.2015.03.040

540 Denning KS, Reinagel P. 2005. Visual Control of Burst Priming in the Anesthetized Lateral
541 Geniculate Nucleus. *J Neurosci* **25**:3531–3538. doi:10.1523/JNEUROSCI.4417-
542 04.2005

543 Desbordes G, Jin J, Weng C, Lesica NA, Stanley GB, Alonso J. 2008. Timing precision in
544 population coding of natural scenes in the early visual system. *PLoS Biol* **6**:e324.
545 doi:10.1371/journal.pbio.0060324

546 Estebanez L, Boustani S El, Destexhe A, Shulz DE. 2012. Correlated input reveals
547 coexisting coding schemes in a sensory cortex. *Nat Neurosci* **15**:1–14.
548 doi:10.1038/nn.3258

549 Guido W, Weyand T. 1995. Burst responses in thalamic relay cells of the awake behaving
550 cat. *J Neurophysiol* **74**:1782–1786.

551 Lesica NA, Jin J, Weng C, Yeh C-I, Butts D a, Stanley GB, Alonso J-M. 2007. Adaptation to
552 stimulus contrast and correlations during natural visual stimulation. *Neuron* **55**:479–91.
553 doi:10.1016/j.neuron.2007.07.013

554 Lesica NA, Stanley GB. 2004. Encoding of natural scene movies by tonic and burst spikes in
555 the lateral geniculate nucleus. *J Neurosci* **24**:10731–40.
556 doi:10.1523/JNEUROSCI.3059-04.2004

557 Martinez-Conde S, Macknik SL, Hubel DH. 2002. The function of bursts of spikes during
558 visual fixation in the awake primate lateral geniculate nucleus and primary visual cortex.
559 *Proc Natl Acad Sci* **99**:13920–13925. doi:10.1073/pnas.212500599

560 McFarland JM, Cui Y, Butts D a. 2013. Inferring nonlinear neuronal computation based on
561 physiologically plausible inputs. *PLoS Comput Biol* **9**:e1003143.
562 doi:10.1371/journal.pcbi.1003143

563 Mease RA, Krieger P, Groh A. 2014. Cortical control of adaptation and sensory relay mode
564 in the thalamus. *Proc Natl Acad Sci U S A* **111**:6798–803.
565 doi:10.1073/pnas.1318665111

566 Mease RA, Kuner T, Fairhall AL, Groh A. 2017. Multiplexed Spike Coding and Adaptation in
567 the Thalamus. *Cell Rep* **19**:1130–1140. doi:10.1016/j.celrep.2017.04.050

568 Newman JP, Fong M-F, Millard DC, Whitmire CJ, Stanley GB, Potter SM. 2015. Optogenetic
569 feedback control of neural activity. *Elife* 1–24. doi:10.7554/eLife.07192

570 Niell CM, Stryker MP. 2010. Modulation of visual responses by behavioral state in mouse
571 visual cortex. *Neuron* **65**:472–9. doi:10.1016/j.neuron.2010.01.033

572 Petersen RS, Brambilla M, Bale MR, Alenda A, Panzeri S, Montemurro M a, Maravall M.
573 2008. Diverse and temporally precise kinetic feature selectivity in the VPm thalamic
574 nucleus. *Neuron* **60**:890–903. doi:10.1016/j.neuron.2008.09.041

575 Poulet JFA, Fernandez LMJ, Crochet S, Petersen CCHH. 2012. Thalamic control of cortical
576 states. *Nat Neurosci* **15**:370–2. doi:10.1038/nn.3035

577 Quiroga RQ, Nadasdy Z, Ben-Shaul Y. 2004. Unsupervised spike detection and sorting with
578 wavelets and superparamagnetic clustering. *Neural Comput* **16**:1661–1687.
579 doi:10.1162/089976604774201631

580 Reinagel P, Godwin D, Sherman SM, Koch C. 1999. Encoding of visual information by LGN
581 bursts. *J Neurophysiol* 2558–2569.

582 Reinhold K, Lien AD, Scanziani M. 2015. Distinct recurrent versus afferent dynamics in
583 cortical visual processing. *Nat Neurosci* **18**. doi:10.1038/nn.4153

584 Rossant C, Kadir SN, Goodman DFM, Schulman J, Belluscio M, Buzsáki G, Harris KD,
585 Hunter MLD, Saleem AB, Grosmark A, Denfield GH, Ecker ASS, Tolias AS, Solomon
586 SG, Carandini M, Belluscio M, Denfield GH, Ecker ASS, Tolias AS, Solomon SG,
587 Buzsáki G, Carandini M, Harris KD. 2015. Spike sorting for large, dense electrode
588 arrays. *Nat Neurosci* 015198. doi:10.1038/nn.4268

589 Schwartz O, Pillow JW, Rust NC, Simoncelli EP. 2006. Spike-triggered neural
590 characterization. *J Vis* **6**:484–507. doi:10.1167/6.4.13

591 Stanley GB. 2002. Adaptive spatiotemporal receptive field estimation in the visual pathway.
592 *Neural Comput* **14**:2925–2946. doi:10.1162/089976602760805340

593 Steriade M, McCormick DA, Sejnowski TJ. 1993. Thalamocortical oscillations in the sleeping
594 and aroused brain. *Science* **262**:679–685. doi:10.1126/science.8235588

595 Suzuki S, Rogawski MA. 1989. T-type calcium channels mediate the transition between tonic
596 and phasic firing in thalamic neurons. *Proc Natl Acad Sci U S A* **86**:7228–7232.
597 doi:10.1073/pnas.86.18.7228

598 Swadlow HA, Gusev AG. 2001. The impact of "bursting" thalamic impulses at a neocortical
599 synapse. *Nat Neurosci* **4**:402–8. doi:10.1038/86054

600 Wang Q, Webber RM, Stanley GB. 2010. Thalamic synchrony and the adaptive gating of
601 information flow to cortex. *Nat Neurosci* **13**:1534–41. doi:10.1038/nn.2670

602 Wang X, Wei Y, Vaingankar V, Wang Q, Koepsell K, Sommer FT, Hirsch J a. 2007.
603 Feedforward Excitation and Inhibition Evoke Dual Modes of Firing in the Cat's Visual
604 Thalamus during Naturalistic Viewing. *Neuron* **55**:465–478.
605 doi:10.1016/j.neuron.2007.06.039

606 Whitmire CJ, Millard DC, Stanley GB. 2017. Thalamic state control of cortical paired-pulse
607 dynamics. *J Neurophysiol* **117**:jn 00415 2016. doi:10.1152/jn.00415.2016

608 Whitmire CJ, Waiblinger C, Schwarz C, Stanley GB. 2016. Information Coding through
609 Adaptive Gating of Synchronized Thalamic Bursting. *CellReports* **14**:1–13.
610 doi:10.1016/j.celrep.2015.12.068

611 Wimmer RD, Schmitt LI, Davidson TJ, Nakajima M, Deisseroth K, Halassa MM. 2015.
612 Thalamic control of sensory selection in divided attention. *Nature*.
613 doi:10.1038/nature15398

614 Wolfart J, Debay D, Le Masson G, Destexhe A, Bal T. 2005. Synaptic background activity
615 controls spike transfer from thalamus to cortex. *Nat Neurosci* **8**:1760–7.
616 doi:10.1038/nn1591

617